Clinical Cancer Research

TIM-3 Dictates Functional Orientation of the Immune Infiltrate in Ovarian Cancer

Jitka Fucikova[1,2], Jana Rakova[2], Michal Hensler[2], Lenka Kasikova[1,2], Lucie Belicova[2], Kamila Hladikova[1,2], Iva Truxova[1,2], Petr Skapa[3], Jan Laco[4], Ladislav Pecen[2], Ivan Praznovec[5], Michael J. Halaska[6], Tomas Brtnicky[7], Roman Kodet[3], Anna Fialova[2], Josephine Pineau[8,9], Alain Gey[8,9], Eric Tartour[8,9], Ales Ryska[4], Lorenzo Galluzzi[10,11,12,13], and Radek Spisek[1,2]

Abstract

Purpose: In multiple oncological settings, expression of the coinhibitory ligand PD-L1 by malignant cells and tumor infiltration by immune cells expressing coinhibitory receptors such as PD-1, CTLA4, LAG-3, or TIM-3 conveys prognostic or predictive information. Conversely, the impact of these features of the tumor microenvironment on disease outcome among high-grade serous carcinoma (HGSC) patients remains controversial.

Experimental Design: We harnessed a retrospective cohort of 80 chemotherapy-naïve HGSC patients to investigate PD-L1 expression and tumor infiltration by $CD8^+$ T cells, $CD20^+$ B cells, DC-$LAMP^+$ dendritic cells as well as by PD-1^+, CTLA4^+, LAG-3^+, and TIM-3^+ cells in relation with prognosis and function orientation of the tumor microenvironment. IHC data were complemented with transcriptomic and functional studies on a second prospective cohort of freshly resected HGSC samples. *In silico* analysis of publicly available RNA expression data from 308 HGSC samples was used as a confirmatory approach.

Results: High levels of PD-L1 and high densities of PD-1^+ cells in the microenvironment of HGSCs were strongly associated with an immune contexture characterized by a robust T_H1 polarization and cytotoxic orientation that enabled superior clinical benefits. Moreover, PD-1^+TIM-$3^+$$CD8^+$ T cells presented all features of functional exhaustion and correlated with poor disease outcome. However, although PD-L1 levels and tumor infiltration by TIM-3^+ cells improved patient stratification based on the intratumoral abundance of $CD8^+$ T cells, the amount of PD-1^+ cells failed to do so.

Conclusions: Our data indicate that PD-L1 and TIM-3 constitute prognostically relevant biomarkers of active and suppressed immune responses against HGSC, respectively.

Introduction

The composition, localization, and functional orientation of the immunologic tumor microenvironment (TME) exhibit considerable degrees of variation, not only across patients, cancer types, and disease stages, but also across distinct metastatic lesions of the same primary tumor (1). Although little is known on how the immunologic profile of metastatic lesions affects disease outcome, in a large number of oncological indications, the immunologic configuration of the primary tumor bears robust prognostic or predictive information (2). For instance, high levels of the coinhibitory molecule CD274 (best known as PD-L1) predict (at least to some extent) the sensitivity of non–small cell lung cancer (NSCLC) patients to immune-checkpoint blockers targeting PD-L1 or its cognate receptor, i.e., programmed cell death 1 (PDCD1, best known as PD-1; refs. 3, 4). Moreover, abundant infiltration by $CD8^+$ cytotoxic T lymphocytes (CTL) as well as signs of a T_H1-polarized immune response is associated with improved disease outcome in a variety of tumors (2, 5–7). However, little is known about the impact of PD-L1 levels and tumor infiltration by immune cells expressing PD-1 and other coinhibitory receptors such as cytotoxic T lymphocyte-associated protein 4 (CTLA4), lymphocyte activating 3 (LAG-3), or hepatitis A virus cellular receptor 2 (HAVCR2, best known as TIM-3) on disease outcome in high-grade serous carcinoma (HGSC) patients.

On the one hand, Hamanishi and colleagues reported that PD-L1 expressed by cancer cells negatively correlates with limited

[1]Department of Immunology, Charles University, 2nd Faculty of Medicine and University Hospital Motol, Prague, Czech Republic. [2]Sotio, Prague, Czech Republic. [3]Department of Pathology and Molecular Medicine, Charles University, 2nd Faculty of Medicine and University Hospital Motol, Prague, Czech Republic. [4]The Fingerland Department of Pathology, Charles University, Faculty of Medicine and University Hospital Hradec Kralove, Czech Republic. [5]Department of Gynecology and Obstetrics, Charles University, Faculty of Medicine and University Hospital Hradec Kralove, Czech Republic. [6]Department of Gynecology and Obstetrics, Charles University, 3rd Faculty of Medicine and University Hospital Kralovske Vinohrady, Prague, Czech Republic. [7]Department of Gynecology and Obstetrics, Charles University, 2nd Faculty of Medicine and University Hospital Motol, Prague, Czech Republic. [8]INSERM U970, Université Paris Descartes, Sorbonne Paris-Cité, Paris, France. [9]Service d'Immunologie Biologique, AP-HP, Hopital Européen Georges Pompidou, Paris, France. [10]Department of Radiation Oncology, Weill Cornell Medical College, New York, New York. [11]Sandra and Edward Meyer Cancer Center, New York, New York. [12]Department of Dermatology, Yale School of Medicine, New Haven, Connecticut. [13]Université Paris Descartes/Paris V, Paris, France.

Note: Supplementary data for this article are available at Clinical Cancer Research Online (http://clincancerres.aacrjournals.org/).

L. Galluzzi and R. Spisek share senior authorship of this article.

Corresponding Author: Jitka Fucikova, Charles University and Sotio, V Uvalu 84, Prague, 150 00, Czech Republic. Phone: 42-022-417-5114; Fax: 42-022-417-5114; E-mail: fucikova@sotio.com

Clin Cancer Res 2019;25:4820–31

doi: 10.1158/1078-0432.CCR-18-4175

©2019 American Association for Cancer Research.

Downloaded from http://aacrjournals.org/clincancerres/article-pdf/25/15/4820/2051487/4820.pdf by guest on 23 May 2025

Translational Relevance

The precise impact of PD-L1 expression levels and infiltration by PD-1$^+$, CTLA4$^+$, LAG-3$^+$, and TIM-3$^+$ T cells on the immunologic configuration of the tumor microenvironment in high-grade serous carcinoma (HGSC) has not yet been determined. Similarly, how these immunologic parameters influence survival in chemotherapy-naïve patients with HGSC undergoing curative surgery remains an open conundrum. Here, we demonstrate that elevated levels of PD-L1 in malignant cells as well as robust infiltration by PD-1$^+$, CTLA4$^+$, or LAG-3$^+$ T cells are not indicative of T-cell exhaustion in patients with HGSC, but rather point to an ongoing IFNγ-dependent immune response with beneficial effects. Conversely, abundant infiltration by TIM-3$^+$ is associated with poor disease outcome, indicating that TIM-3 has a prominent role in limiting immune responses against HGSCs. Our data suggest that TIM-3 inhibitors should be tested as neoadjuvant or adjuvant agents for the management of chemotherapy-naïve patients with HGSC.

infiltration by immune effector cells and hence poor disease outcome, reflecting the largely immunosuppressive activity of this molecule (8). On the other hand, various reports demonstrate that PD-L1 expression as a consequence of interferon gamma (IFNG, best known as IFNγ) signaling is associated with strong infiltration by CD8$^+$ CTLs, representing a mechanism of compensation against a therapeutically beneficial tumor-targeting immune response (9–13). Similarly, although some reports attribute to robust infiltration by PD-1$^+$ cells a negative prognostic value, potentially linked to the highly exhausted status of these cells (14–16), other studies point to a rather beneficial effect (17, 18), perhaps linked to the fact that CD103$^+$PD-1$^+$CD8$^+$ T cells appear to retain functional competence in the ovarian TME (19). We have recently demonstrated that CD20$^+$ B cells and DC-LAMP$^+$ dendritic cells (DC) infiltrating HGSC lesions have a positive prognostic value as they orchestrate a T_H1-polarized immune response coupled to abundant CD8$^+$ CTL infiltration (5). However, the specific effect of PD-L1 levels and infiltration by immune cells expressing coinhibitory receptors on the composition and functional orientation of the TME in ovarian cancer patients, and how this influences disease outcome, remains to be clarified.

Here, we demonstrate that both elevated PD-L1 levels and high densities of PD-1$^+$ cells in the HGSC TME are strongly associated with robust T_H1 polarization and cytotoxic orientation that enable superior clinical benefits, but only the former can be used to improve patient stratification based on the intratumoral abundance of CD8$^+$ T cells. Conversely, not only CD8$^+$ CTLs coexpressing PD-1 and TIM-3 present all the features of functional exhaustion, but their abundance has a negative independent prognostic value. Our data demonstrate that immunosuppression in the TME of therapy-naïve HGSC patients is dictated mainly by TIM-3.

Materials and Methods

Patients

Study group 1. A retrospective series of 80 formalin-fixed paraffin-embedded (PPFE) samples were obtained from patients with HGSC who underwent primary surgery in the absence of neoadjuvant chemotherapy between 2008 and 2014 at University Hospital Hradec Kralove (Czech Republic). Baseline characteristics of these patients are summarized in Table 1. Pathology staging was performed according to the 8th TNM classification (2017), and histologic types were determined according to the current WHO classification (20, 21). Data on long-term clinical outcome were obtained retrospectively by interrogation of municipality registers or families. The protocol was approved by the local ethics committee (reference number 201607 S14P).

Table 1. Main clinical and biological characteristic of study group 1

Variable	Overall cohort ($n = 80$)
Age	
Mean age (y) ± SEM	61 ± 10
Range	41–79
pTNM stage	
Stage I	20 (25%)
Stage II	7 (8.7%)
Stages III and IV	53 (66.3%)
Debulking	
R0	39 (48.5%)
R1	4 (5%)
R2	37 (46.3%)
Vital status of patients	
Alive	35 (43.7%)
Death	45 (56.3%)

Study group 2. An additional series of 20 samples from HGSC patients was prospectively collected at University Hospital Motol (Prague, Czech Republic). This study was conducted in accordance with the Declaration of Helsinki and the protocol was approved by the local ethics committee (Progress UK, Q40/11). Written informed consent was obtained from patients before inclusion in the study. Baseline characteristics of these patients are summarized in Supplementary Table S1. The experimental design of the study is summarized in Supplementary Fig. S1.

IHC

As previously described, tumor specimens from study group 1 were fixed in neutral buffered 10% formalin solution and embedded in paraffin as per standard procedures (5). Immunostaining with antibodies specific for programmed cell death 1 (PDCD1, best known as PD1), CD274 (best known as PD-L1), lymphocyte activating gene 3 (LAG-3), cytotoxic T lymphocyte-associated protein 4 (CTLA4), lysosomal associated membrane protein 3 (LAMP3; best known as DC-LAMP), CD8, and CD20 was performed according to conventional protocols (Supplementary Table S2). Briefly, tissue sections were deparaffinized, followed by antigen retrieval with Target Retrieval Solution (Leica) at pH 6.0 (for PD-L1), in TRIS EDTA pH 9.0 (for CTLA4, LAG-3, and PD-1) or pH 8.0 (for CD8, CD20, and DC-LAMP) in preheated water bath (98°C, 30 minutes). Sections were allowed to cool down to room temperature for 30 minutes, and endogenous peroxidase and alkaline phosphatase was blocked with 3% H_2O_2, levamisole, and blocking solution Bloxall (Vector), respectively, for 15 minutes. Thereafter, sections were treated with protein block (DAKO) for 15 minutes and incubated with primary antibodies, followed by the revelation of enzymatic activity. Sections were counterstained with hematoxylin (DAKO)

Downloaded from http://aacrjournals.org/clincancerres/article-pdf/25/15/4820/2051487/4820.pdf by guest on 23 May 2025

for 30 seconds. Images were acquired using a Leica Aperio AT2 scanner (Leica).

Cell quantification

PD-1$^+$, CTLA4$^+$, and LAG-3$^+$ cells were differentially quantified in the stroma and tumor nests of whole tumor sections with Calopix software (Tribvn). As previously described, the density of CD8$^+$ T cells, DC-LAMP$^+$ DCs, and CD20$^+$ B cells was quantified in the entire TME (5). Data are reported as the absolute number of positive cells/mm^2 (for PD-1$^+$, CTLA4$^+$, LAG-3$^+$, DC-LAMP$^+$, CD8$^+$ cells) or cell surface/tumor section surface (for CD20$^+$ cells). PD-L1 expression was scored in the intratumoral and stromal compartments as a percentage of tumor area and categorized as 1 (0%), 2 (1%–4%), 3 (5%–9%), and 4 (>10%), as previously described (22). Quantitative assessments were performed by three independent investigators (J. Fucikova, J. Rakova, L. Belicova) and reviewed by an expert pathologist (J. Laco and P. Skapa).

Flow cytometry

As previously described, total live mononuclear cells were isolated from fresh tumor specimens (5). Mononuclear cells were stained with multiple panels of fluorescent primary antibodies (Supplementary Table S3) or appropriate isotype controls for 20 minutes at 4°C in the dark, followed by washing and acquisition on a Fortessa flow cytometer (BD Biosciences). Flow cytometry data were analyzed with the FlowJo software (TreeStar).

Degranulation and IFNγ production after anti–PD-1 and anti–TIM-3 cultivation and *in vitro* stimulation

Mononuclear cells isolated from fresh tumor specimens (study group 2) were incubated with 10 μg/mL anti–PD-1, 10 μg/mL anti–TIM-3, and combination of both antibodies for 24 hours in 37°C and 5% CO_2. After cultivation, mononuclear cells were stimulated with 50 ng/mL phorbol 12-myristate 13-acetate (PMA) + 1 μg/mL ionomycin in the presence of anti-CD107a FITC monoclonal antibody (BioLegend) for 1 hour followed by 3-hour incubation with brefeldin A (BioLegend). Unstimulated cells were used as control. Cells were then washed in PBS, stained with anti-CD45 PerCP (EXBIO), anti-CD3 Alexa Fluor 700 (EXBIO), anti-CD4 ECD (Beckman Coulter), and anti-CD8 HV500 (BD Biosciences) monoclonal antibodies, fixed in fixation/permeabilization buffer (eBioscience), permeabilized with permeabilization buffer (eBioscience), and intracellularly stained with anti-IFNγ PE-Cy7 (eBioscience) monoclonal antibody. Flow cytometry was performed on the LSRFortessa analyzer, and data were analyzed with the FlowJo software package (Supplementary Fig. S6B; Tree Star, Inc.).

Next-generation sequencing data analysis

As previously described, hierarchical clustering analysis was conducted for differentially expressed genes (DEG) using the PHEATMAP package in R, based on the Euclidean distance and complete clustering method (5). The MCP-counter R package was used to estimate the abundance of tissue-infiltrating immune cell populations (Supplementary Table S4; ref. 23).

The Cancer Genome Atlas (TCGA) data analysis

Patients with HGSC ($n = 308$) were identified in TCGA public database (https://cancergenome.nih.gov/). DEGs between the *PD-L1*^{Hi} and *PD-L1*^{Lo} groups were determined using the LIMMA-R package (24). Hierarchical clustering analysis was conducted using the ComplexHeatmap package, based on the Euclidean distance and complete clustering method (25). Immune analyses were performed using ClueGo (26). The MCP-counter R package was used to estimate the abundance of tissue-infiltrating immune cell populations (23).

In situ immunofluorescence of tumor-infiltrating lymphocytes

Tumor specimens from study group 1 were fixed in neutral buffered 10% formalin solution and embedded in paraffin as per standard procedures. Sections were therefore subjected to indirect immunofluorescence based on nonlabeled primary antibodies specific for PD-1, TIM-3, and CD8 coupled to appropriate HRP-polymer secondary antibodies, followed by Tyramide Signal Amplification reagents with fluorescent dyes (Supplementary Table S5). Isotype-matched antibodies were used as negative controls and DAPI-containing mounting medium (DAKO) was used for nuclear counterstaining.

Image analysis and automated cell count

Stained sections were imaged with an automated Vectra microscope (PerkinElmer), followed by analysis by inForm software (PerkinElmer) as described previously in detail (27). Data are reported as means of positive cells from 5 imaging fields acquired using a 20× objective. An independent operator and an expert pathologist confirmed phenotyping by visual inspection. In particular, each phenotyping image was double checked to minimize the risk of false determinations owing to potential overlaps in fluorescence and interoperator variance.

Statistical analysis

As previously described, survival analysis was performed using the Survival R package, using both log-rank tests and Cox proportional hazard regressions (5). For log-rank tests, the prognostic value of continuous variables was assessed using median cutoffs. For Cox proportional hazard regressions, cell densities were log-transformed. In multivariate Cox regressions, variables that were not significantly associated with prognosis in univariate analysis were not included, as well as variables intrinsically correlated. Cox proportional hazard regression analysis, log-rank analysis, Fisher exact tests, Student *t* tests, and the Wilcoxon and Mann–Whitney tests were used to assess statistical significance, *P* values are reported (considered not significant when >0.05).

Results

Tumor infiltration by CD8$^+$ T lymphocytes, CD20$^+$ B cells, and DC-LAMP$^+$ DCs correlate with prolonged survival in patients with HGSC

Tumor samples from a retrospective series of 80 patients with HGSC who did not receive neoadjuvant chemotherapy (study group 1; Table 1) were analyzed for the densities of CD8$^+$ T cells, CD20$^+$ B cells, and DC-LAMP$^+$ DCs by IHC (Supplementary Fig. S2A). As published previously by our group, HGSC patients with high density of CD8$^+$ T cells (CD8^{Hi}), CD20$^+$ B cells (CD20^{Hi}), and DC-LAMP$^+$ DCs (DC-LAMP^{Hi}) exhibited significantly longer relapse-free survival (RFS) and overall survival (OS) as compared with their low counterparts (CD8$^+$ T cells RFS: $P = 0.03$, OS $P = 0.01$; CD20$^+$ B cells RFS: $P = 0.02$, OS $P = 0.02$; DC-LAMP$^+$ DCs RFS: $P = 0.0001$, OS $P < 0.0001$; Supplementary Fig. S2B and S2C). To assess whether infiltration by either CD20$^+$ B cells or

Downloaded from http://aacrjournals.org/clincancerres/article-pdf/25/15/4820/2051487/4820.pdf by guest on 23 May 2025

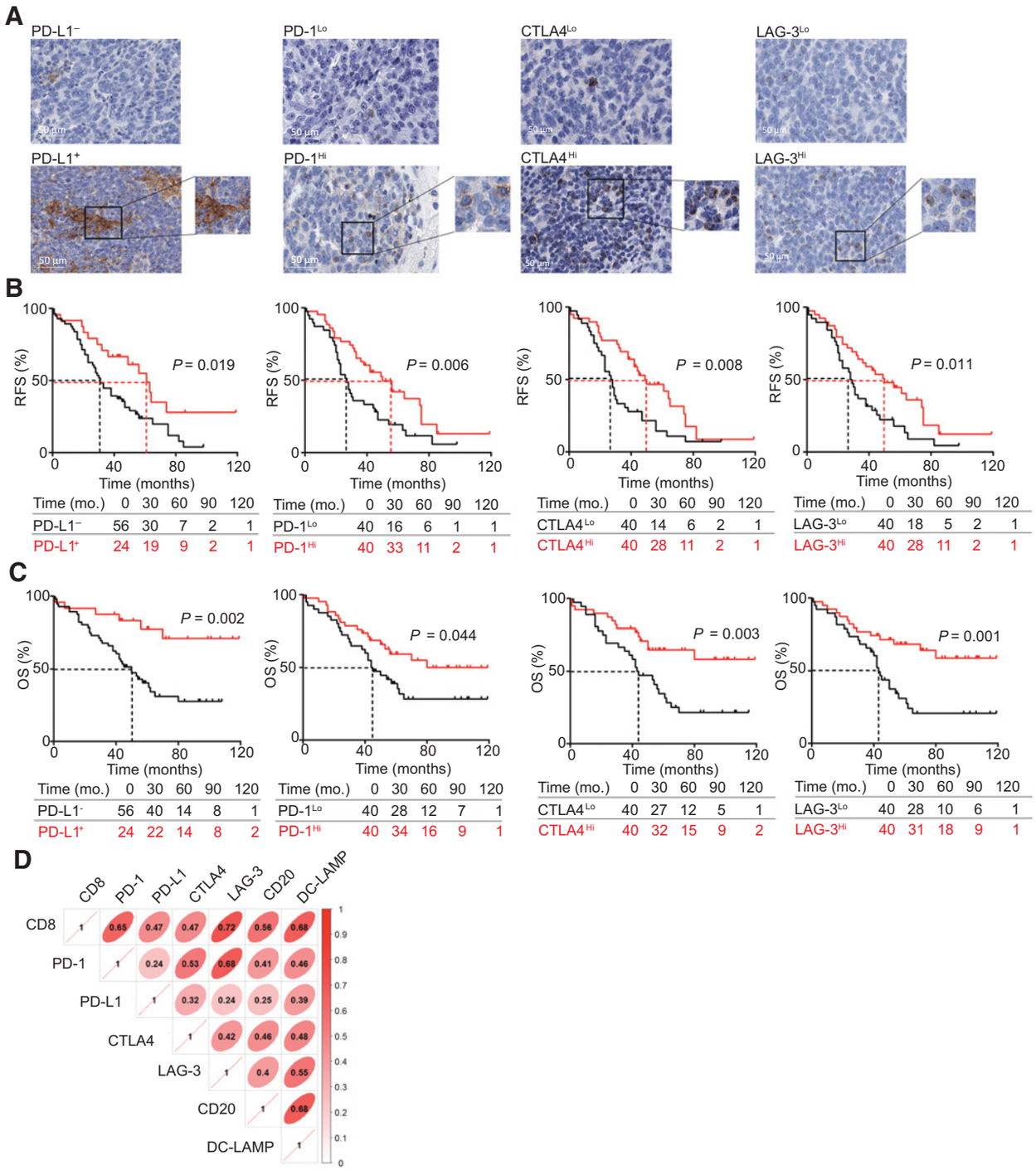

Figure 1.

Prognostic impact of PD-L1$^+$, PD-1$^+$, CTLA4$^+$, and LAG-3$^+$ cells in the TME of chemotherapy-naïve HGSC patients. **A,** Representative images of PD-L1, PD-1, CTLA4, and LAG-3 immunostaining. Scale bar, 50 μm. RFS (**B**) and OS (**C**) of 80 patients with HGSC (study group 1) who did not receive neoadjuvant chemotherapy, upon stratifying patients based on a cutoff of 5% malignant cells with PD-L1 expression and median density of PD-1$^+$, CTLA4$^+$, and LAG-3$^+$ cells in the tumor nests. Survival curves were estimated by the Kaplan–Meier method, and differences between groups were evaluated using the log-rank test. The number of patients at risk is reported. **D,** The correlation matrix for CD8$^+$, PD-1$^+$, PD-L1$^+$, CTLA4$^+$, LAG-3$^+$, CD20$^+$, and DC-LAMP$^+$ cells in the tumor nest of HGSC patients (study group 1).

Downloaded from http://aacrjournals.org/clincancerres/article-pdf/25/15/4820/2051487/4820.pdf by guest on 23 May 2025

DC-LAMP$^+$ DCs would improve the prognostic value of intratumoral CD8$^+$ T cells only, we evaluated RFS and OS upon stratifying patients from study group 1 into four subsets for each marker (CD8^{Hi}/CD20^{Hi}, CD8^{Hi}/CD20^{Lo}, CD8^{Lo}/CD20^{Hi}, and CD8^{Lo}/CD20^{Lo} and CD8^{Hi}/DC-LAMP^{Hi}, CD8^{Hi}/DC-LAMP^{Lo}, CD8^{Lo}/DC-LAMP^{Hi}, and CD8^{Lo}/DC-LAMP^{Lo}). Indeed both CD8^{Hi}/CD20^{Hi} and CD8^{Hi}/DC-LAMP^{Hi} patients exhibited improved OS as compared with their CD8^{Hi}/CD20^{Lo} and CD8^{Hi}/DC-LAMP^{Lo} counterparts ($P = 0.006$ and $P = 0.005$, respectively; Supplementary Fig. S2D and S2E). These data confirm previous findings from our group indicating that a high density of tumor-infiltrating CD8$^+$ T cells, CD20$^+$ B cells, and DC-LAMP$^+$ DCs correlates with improved disease outcome in chemotherapy-naïve HGSC patients, and that the density of CD20$^+$ B cells and DC-LAMP$^+$ DCs can be harnessed to identify CD8^{Hi} patients with relatively poor OS (5).

Table 2. Univariate Cox proportional hazard analysis

	OS	
Variable	HR (95% CI)	*P*
Stage 2	0.5 (0.058–4.25)	0.523
Stage 3	3.87 (1.51–9.9)	**0.004**
Stage 4	5.34 (1.27–22.4)	**0.022**
Age	1 (1–1.1)	**0.04**
Debulking R1	1.24 (0.29–5.43)	**0.02**
Debulking R2	2.14 (1.13–4.03)	**0.02**
CA125	1.00 (1.00–1.00)	0.14
PD-1	0.98 (0.96–1.00)	0.10
PD-L1	0.28 (0.12–0.67)	**0.004**
CTLA4	0.89 (0.8–0.98)	**0.017**
LAG-3	0.98 (0.95–1.00)	0.084
TIM-3	1.03 (1.00–1.06)	**0.04**
CD8	1 (1.00–1.00)	**0.017**
DC-LAMP	0.86 (0.76–0.97)	**0.014**
CD20	0.23 (0.05–1.00)	**0.05**

Activation of immune checkpoints correlates with improved disease outcome in HGSC patients

To elucidate the prognostic impact of immune-checkpoint status among chemotherapy-naïve HGSC patients, tumor samples from study group 1 (Table 1) were analyzed for the expression of PD-L1 in the tumor nest, as well as for the density of PD-1$^+$, CTLA4$^+$, and LAG-3$^+$ cells by IHC (Fig. 1A; Supplementary Figs. S3 and S4). PD-L1 levels as well as infiltration by PD-1$^+$, CTLA4$^+$, and LAG-3$^+$ cells were heterogeneous across samples but did not differ based on the site of assessment (tumor stroma vs. tumor nests; Supplementary Fig. S5A) and pathologic disease stage (Supplementary Fig. S5B).

To assess the prognostic impact of PD-L1 expression in the TME, we evaluated RFS and OS upon stratifying patients (study group 1) based on a cutoff of 5% malignant cells with membranous PD-L1 expression, which is currently used in the clinic to identify patients eligible for PD-1/PD-L1 targeting immune-checkpoint blockers (28). Patients with PD-L1$^+$ tumor nests (24 out of 80 patients) had prolonged RFS and OS as compared with their PD-L1$^-$ counterparts (RFS: $P = 0.019$; OS: $P = 0.002$; Fig. 1B and C). Univariate Cox regression analysis confirmed a strong prognostic impact for PD-L1 expression in tumor nests [hazard ratio (HR) = 0.28; 95% confidence interval = 0.12–0.67; $P = 0.004$; Table 2], and the significance of this association was confirmed by multivariate analysis (HR = 0.3; 95% confidence interval = 0.12–0.61; $P = 0.007$; Table 3). These data suggest that high PD-L1 levels in the TME may be indicative of an ongoing immune response that favorably affects disease outcome among HGSC patients, regardless of the stage of the disease.

Next, we investigated RFS and OS upon stratifying study group 1 based on the median density of PD-1$^+$, CTLA4$^+$, or LAG-3$^+$ cells infiltrating tumor nests (Fig. 1A; Supplementary Figs. S3 and S4). Patients with high density of PD-1$^+$ cells (PD-1^{Hi}) in their TME exhibited significantly longer RFS and OS as compared with their PD-1^{Lo} counterparts (RFS: $P = 0.006$; OS: $P = 0.044$; Fig. 1B and C). Similar results were obtained when patients were stratified according to the median density of CTLA4$^+$ and LAG-3$^+$ cells (CTLA4 RFS: $P = 0.008$; OS: $P = 0.003$; LAG-3 RFS: $P = 0.011$; OS: $P = 0.001$; Fig. 1B and C). Univariate Cox regression analysis identified a positive prognostic impact only for tumor infiltration by CTLA4$^+$ cells (HR = 0.89; 95% confidence interval = 0.8–0.98; $P = 0.017$; Table 2), which could not be confirmed on multivariate analysis (Table 3). Most likely, these findings reflect the strong correlation between the density of tumor-infiltrating CD8$^+$ T cells and the intratumoral abundance of PD-1$^+$, CTLA4$^+$, and LAG-3$^+$ cells (Fig. 1D), suggesting that PD-1, CTLA4, and LAG-3 largely behave as T-cell markers in this setting.

PD-L1 levels positively correlate with antitumor immunity and improved disease outcome in HGSC

To further characterize the impact of PD-L1 expression on the immunologic profile of HGSCs, we used RNA-seq to compare gene-expression profiles in PD-L1$^-$ vs. PD-L1$^+$ patients. We identified a set of 1,114 genes that were significantly overrepresented in samples from PD-L1$^+$ patients as compared with their PD-L1$^-$ counterparts (Fig. 2A). Functional studies revealed a strong association between such DEGs with immune system activation and inflammation. Alongside, we used the MCP-counter R package to estimate the relative expression levels of different cell populations in the TME of PD-L1$^+$ and PD-L1$^-$ patients. Compared with their PD-L1$^-$ counterparts, PD-L1$^+$ tumors were enriched in gene sets specific for T cells ($P < 0.0001$) and CD8$^+$ T cells ($P < 0.0001$; Fig. 2B). To validate these findings with another technique, we next analyzed the relationship between PD-L1 expression and the intratumoral abundance of CD8$^+$ CTLs by IHC (study group 1). We observed significantly higher densities of CD8$^+$ CTLs infiltrating tumor nests ($P < 0.0001$) in samples from PD-L1$^+$ versus PD-L1$^-$ patients (Fig. 2C). Similar results were obtained for CD20$^+$ B cells and DC-LAMP$^+$ DCs (Fig. 2C), confirming previous results from our group (5). Moreover, to address the functional properties of HGSC-infiltrating CD8$^+$ CTLs from PD-L1$^+$ versus PD-L1$^-$ patients, we performed a flow cytometry analysis on 20 freshly resected HGSCs (study group 2; Supplementary Table S1) on which PD-L1 status had been previously assessed by IHC. We observed significantly higher percentages of CD8$^+$ CTLs expressing IFNγ$^+$ ($P = 0.015$), as well as of CD8$^+$ CTLs coexpressing IFNγ and granzyme B (GZMB, a key CTL effector; $P = 0.044$) or CD107a (a marker of CTL activation; $P = 0.039$), in PD-L1$^+$ versus PD-L1$^-$ patients (Fig. 2D). Moreover, we observed a correlation between *CD274* mRNA levels and *IFNG* mRNA levels ($R = 0.61$;

Table 3. Multivariate Cox proportional hazard analysis

	OS	
Variable	HR (95% CI)	*P*
Stage 4	119.78 (2.18–4518.48)	**0.01**
PD-L1	0.3 (0.12–0.61)	**0.007**
TIM-3	1.41 (1.1–1.9)	**0.03**

Downloaded from http://aacrjournals.org/clincancerres/article-pdf/25/15/4820/2051487/4820.pdf by guest on 23 May 2025

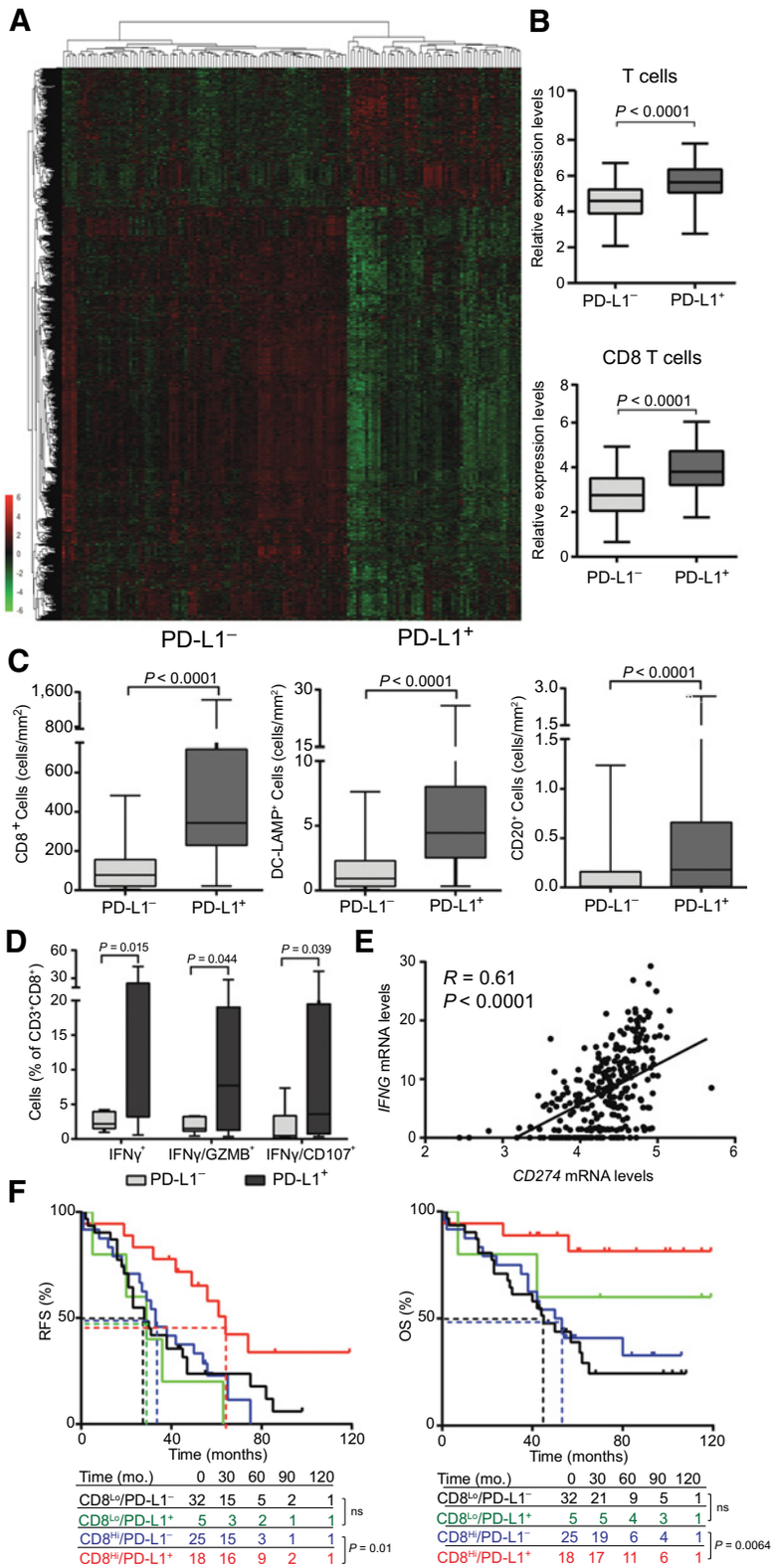

Figure 2.

PD-L1 levels positively correlate with antitumor immunity in HGSC. **A,** Hierarchical clustering of 1,114 genes that were significantly changed in 154 PD-L1$^+$ patients as compared with their 154 PD-L1$^-$ counterparts from the TCGA public database. **B,** Relative expression levels of gene sets associated with T cells and CD8$^+$ T cells across PD-L1$^+$ and PD-L1$^-$ HGSCs, as determined by MCP-counter on RNA-seq data from the TCGA public database. Box plots: lower quartile, median, upper quartile; whiskers, minimum, maximum. **C,** Density of CD8$^+$ T cells, DC-LAMP$^+$ DCs, and CD20$^+$ B cells in the tumor nests in PD-L1$^-$ and PD-L1$^+$ HGSCs ($n = 80$; study group 1). Box plots: lower quartile, median, upper quartile; whiskers, minimum, maximum. **D,** Percentage of IFNγ$^+$, IFNγ$^+$/GZMB$^+$, and IFNγ$^+$/CD107$^+$ cells among CD3$^+$CD8$^+$ cells from the HGSCs of PD-L1$^-$ and PD-L1$^+$ patients after nonspecific stimulation (study group 2). Box plots: lower quartile, median, upper quartile; whiskers, minimum, maximum. **E,** Correlation between the *IFNG* mRNA expression levels and *CD274* mRNA expression in 308 HGSC patients from the TCGA public database. R, Pearson correlation coefficient. **F,** RFS and OS of HGSC patients who did not receive neoadjuvant chemotherapy, upon stratification based on median density of CD8$^+$ T cells and PD-L1 levels (study group 1). Survival curves were estimated by the Kaplan–Meier method, and differences between groups were evaluated using log-rank test. The number of patients at risk is reported.

Downloaded from http://aacrjournals.org/clincancerres/article-pdf/25/15/4820/2051487/4820.pdf by guest on 23 May 2025

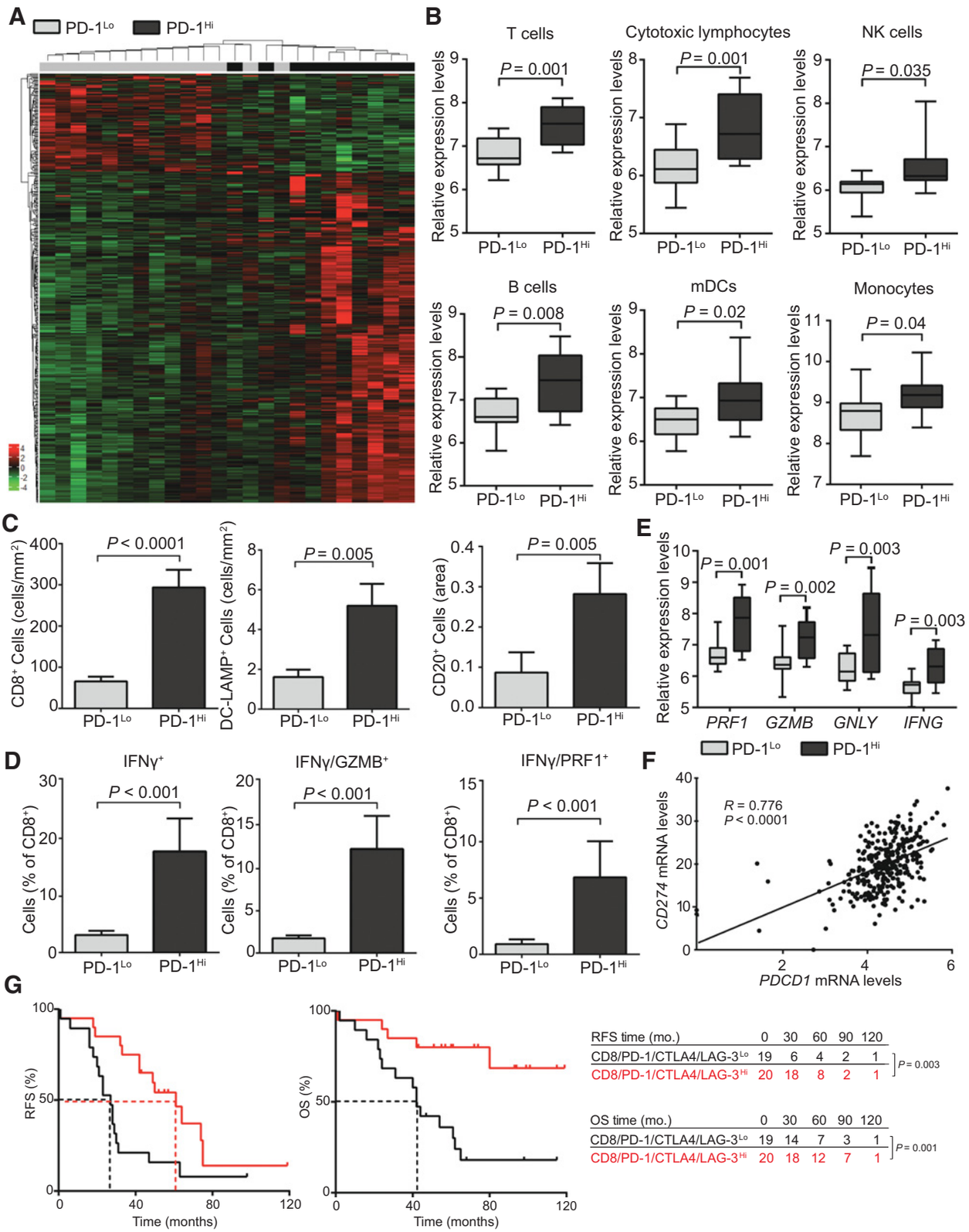

Downloaded from http://aacrjournals.org/clincancerres/article-pdf/25/15/4820/2051487/4820.pdf by guest on 23 May 2025

$P < 0.0001$) in HGSC patients from the TCGA public database (Fig. 2E). Conversely, rIFNγ failed to alter the percentage of PD-L1$^+$, PD-1$^+$, and CTLA4$^+$ CD8$^+$ T cells, irrespective of whether the latter were exposed to rIFNγ alone or in the presence of malignant cells that could or could not engage in physical contacts (study group 2; Supplementary Fig. S6). These findings suggest that IFNγ has limited short-term effect on CD8$^+$ T cells isolated from the tumor microenvironment, but favors PD-L1 expression on malignant cells, in line with previous reports (10).

Because both CD8$^+$ T cells and PD-L1 influence disease outcome in patients with HGSC not receiving neoadjuvant chemotherapy, we assessed RFS and OS upon stratifying patients from study group 1 into four subsets (CD8^{Hi}/PD-L1$^+$, CD8^{Hi}/PD-L1$^-$, CD8^{Lo}/PD-L1$^+$, and CD8^{Lo}/PD-L1$^-$). We found that CD8^{Hi}/PD-L1$^+$ patients had improved RFS and OS as compared with their CD8^{Hi}/PD-L1$^-$ counterparts ($P = 0.01$ and $P = 0.0064$, respectively; Fig. 2F). Importantly, the same did not hold true in the CD8^{Lo} patient subset (Fig. 2F). Taken together, these findings indicate that high PD-L1 levels in the TME of HGSC infiltrated by CD8$^+$ CTLs are indicative of an active IFNγ-dependent immune response that positively influences disease outcome.

Tumor infiltration by PD-1$^+$ cells correlates with improved antitumor immunity in HGSC patients

We performed RNA-sequencing to compare gene-expression profiles from 24 HGSCs from study group 1 for which PD-1 status had been evaluated by IHC. We identified a set of 425 transcripts that are significantly overrepresented in samples from PD-1^{Hi} lesions as compared with their PD-1^{Lo} counterparts (Fig. 3A; Supplementary Table S6). Pathway studies revealed a strong association of such DEGs and immune system activation and inflammation. Alongside, we used the MCP-counter R package to estimate the relative expression levels of gene sets linked to specific immune cell populations in the TME of PD-1^{Hi} versus PD-1^{Lo} patients. Compared with their PD-1^{Lo} counterparts, PD-1^{Hi} HGSCs exhibited overrepresentation of gene sets specific for T cells ($P = 0.001$), cytotoxic lymphocytes ($P = 0.001$), NK cells ($P = 0.035$), B cells ($P = 0.008$), DCs ($P = 0.02$), and monocytes ($P = 0.04$; Fig. 3B). Next, we performed IHC to obtain further insights into the links between PD-1$^+$ cell infiltration and the abundance of CD8$^+$ CTLs, DC-LAMP$^+$ DCs, and CD20$^+$ B cells in HGSC samples (study group 1). We observed higher densities of CD8$^+$ T cells ($P < 0.0001$), DC-LAMP$^+$ DCs ($P = 0.005$), and CD20$^+$ B cells ($P = 0.005$) in the TME of PD-1^{Hi} patients as compared with their PD-1^{Lo} counterparts (Fig. 3C; Supplementary Fig. S7), corroborating the notion that PD-1^{Lo} lesions have a scarce immune infiltrate. To investigate the functional profile of CD8$^+$ CTLs from PD-1^{Hi} versus PD-1^{Lo} HGSCs, we harnessed study group 2 (Supplementary Table S1) to perform flow cytometry on freshly resected samples that were also previously scored for PD-1$^+$ cell infiltration by IHC. PD-1^{Hi} lesions contained a significantly higher percentage of CD8$^+$ CTLs staining positively for IFNγ ($P < 0.001$), IFNγ and GZMB ($P < 0.001$), and IFNγ and perforin 1 (PRF1, another T-cell effector molecule; $P < 0.001$) upon nonspecific activation *ex vivo*, as compared with their PD-1^{Lo} counterparts (Fig. 3D). Consistently, the mRNAs coding for multiple CD8$^+$ T-cell effector molecules including *IFNG*, *PRF1*, *GZMB*, and *GNLY* were overrepresented in PD-1^{Hi} versus PD-1^{Lo} HGSCs, as determined by RNA-sequencing in study group 1 (Fig. 3E). Moreover, we found a strong correlation between the transcripts coding for PD-1 (*PDCD1*) and PD-L1 (*CD274*) ($R = 0.776$; $P < 0.0001$) in HGSC patients from the TCGA database (Fig. 3F). However, stratifying patients from Study group 1 into four subsets based on the frequency of tumor-infiltrating CD8$^+$ T cells and PD-1$^+$ cells (CD8^{Hi}/PD-1^{Hi}, CD8^{Hi}/PD-1^{Lo}, CD8^{Lo}/PD-1^{Hi}, and CD8^{Lo}/PD-1^{Lo}) failed to ameliorate the prognostic assessment provided by tumor-infiltrating CD8$^+$ T cells only (Supplementary Fig. S8A). This is in line with (i) the fact that the density of tumor-infiltrating PD-1$^+$ cells had no prognostic value in multivariate analyses (Table 3); (ii) and the robust correlation between the density of tumor-infiltrating PD-1$^+$ and CD8$^+$ cells (Fig. 1D), which is also evident when the sizes of CD8^{Hi}/PD-1^{Hi}, CD8^{Hi}/PD-1^{Lo}, CD8^{Lo}/PD-1^{Hi}, and CD8^{Lo}/PD-1^{Lo} groups are compared (Supplementary Fig. S8A). The same applies to costratification based on CD8 and LAG-3 (study group 1; Supplementary Fig. S8B). Conversely, the density of tumor-infiltrating CTLA4$^+$ cells behaves as PD-L1 levels in that CD8^{Hi}/CTLA4^{Hi} patients had improved RFS and OS compared with their CD8^{Hi}/CTLA4^{Lo} counterparts ($P = 0.06$ and $P = 0.002$, respectively; study group 1; Supplementary Fig. S8C). Notably, PD-L1 levels and infiltration by CTLA4$^+$ cells were the two parameters investigated in this study with lowest degree of correlation with the intratumoral abundance of CD8$^+$ T cells (Fig. 1D), indicating that low CTLA4 expression can be harnessed to identify CD8^{Hi} HGSC patients with relatively poor disease outcome.

Finally, we evaluated the combined prognostic value of tumor infiltration by CD8$^+$, PD-1$^+$, CTLA4$^+$, and LAG-3$^+$ cells by stratifying study group 1 in two groups of patients based on high or low density of all parameters. Not surprisingly, patients with high levels of HGSC-infiltrating CD8$^+$, PD-1$^+$, CTLA4$^+$, and LAG-3$^+$ cells had superior RFS and OS as compared with their low counterparts ($P = 0.003$ and $P = 0.001$, respectively; Fig. 3G).

Downloaded from http://aacrjournals.org/clincancerres/article-pdf/25/15/4820/2051487/4820.pdf by guest on 23 May 2025

Figure 3.

Tumor infiltration by PD-1$^+$ cells correlates with improved antitumor immunity in HGSC patients. **A,** Hierarchical clustering of 425 transcripts that were significantly changed in 12 PD-1^{Hi} patients as compared with their 12 PD-1^{Lo} counterparts, as determined by RNA-sequencing (study group 1). **B,** Relative expression levels of gene sets associated with T cells, CD8$^+$ T cells, NK cells, B cells, mDCs, and monocytes across PD-1^{Hi} and PD-1^{Lo} HGSCs, as determined by MCP-counter on RNA-seq data from study group 1. Box plots: lower quartile, median, upper quartile; whiskers, minimum, maximum. **C,** Density of CD8$^+$ T cells, DC-LAMP$^+$ DCs, and CD20$^+$ B cells in the tumor nests in PD-1^{Lo} and PD-1^{Hi} HGSCs from study group 1 ($n = 80$). Box plots: lower quartile, median, upper quartile; whiskers, minimum, maximum. **D,** Percentage of IFNγ$^+$, IFNγ$^+$/GZMB$^+$, and IFNγ$^+$/PRF1$^+$ cells among CD3$^+$CD8$^+$ cells from the 20 HGSCs of PD-1^{Lo} and PD-1^{Hi} patients after nonspecific stimulation (study group 2). Box plots: lower quartile, median, upper quartile; whiskers, minimum, maximum. **E,** Relative expression levels of *PRF1, GZMB, GNLY,* and *IFNG* in 154 PD-1^{Lo} and 154 PD-1^{Hi} HGSCs from the TCGA public database, as determined by RNA-seq. plots: lower quartile, median, upper quartile; whiskers, minimum, maximum. **F,** Correlation between the *PDCD1* mRNA expression levels and *CD274* mRNA expression in 308 HGSC patients from the TCGA public database. R, Pearson correlation coefficient. **G,** RFS and OS of 80 HGSC patients from study group 1 who did not receive neoadjuvant chemotherapy, upon stratification based on median density of CD8$^+$, PD-1$^+$, CTLA4$^+$, and LAG-3$^+$ cells in tumor nests. Survival curves were estimated by the Kaplan–Meier method, and differences between groups were evaluated using the log-rank test. The number of patients at risk are reported.

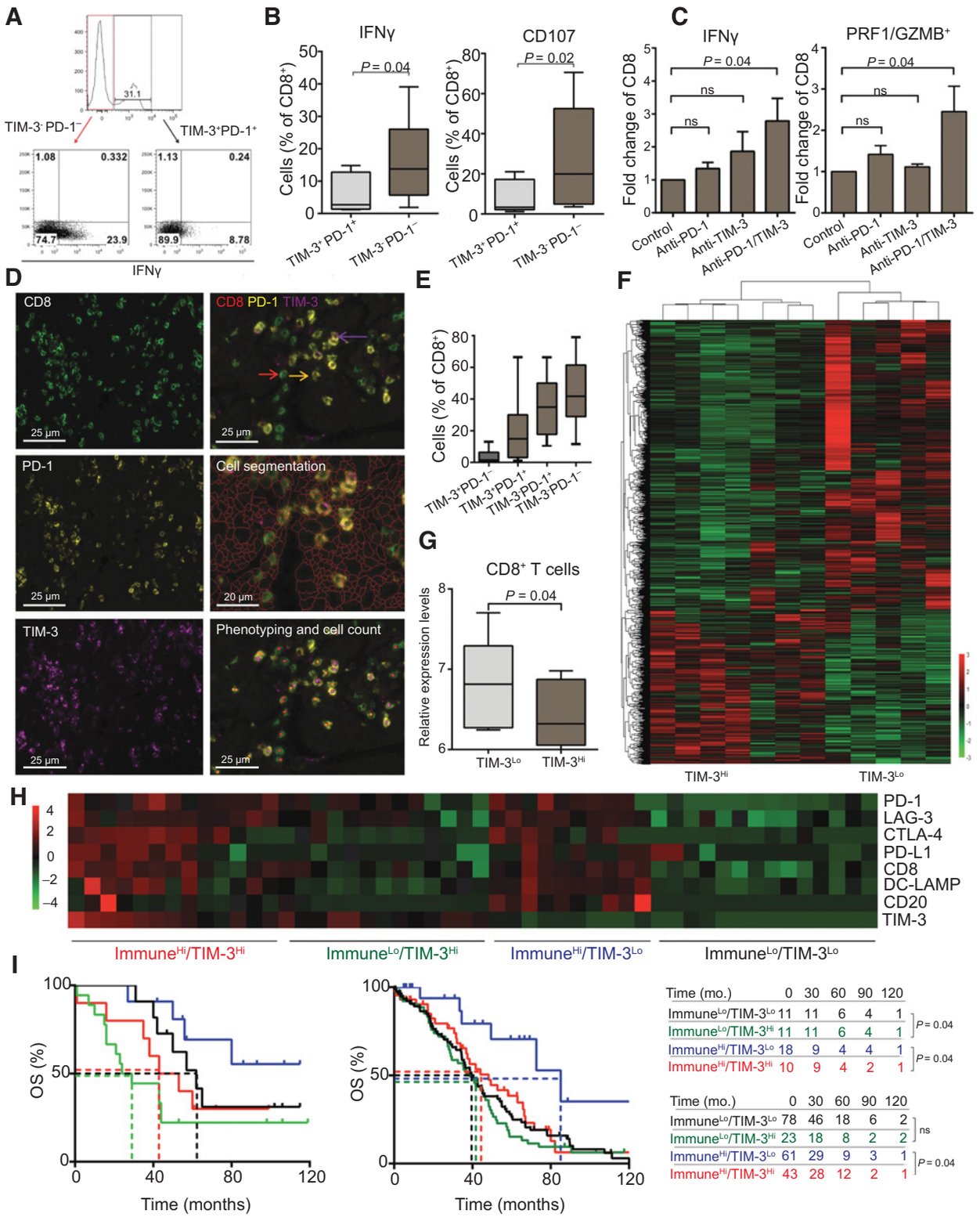

Downloaded from http://aacrjournals.org/clincancerres/article-pdf/25/15/4820/2051487/4820.pdf by guest on 23 May 2025

TIM-3 dictates clinically relevant immunosuppression in the TME of HGSCs

We were surprised by the fact that neither the PD-1/PD-L1 axis, neither CTLA4, nor LAG-3 appears to mediate clinically relevant immunosuppressive effects in the TME of chemotherapy-naïve HGSC patients (Figs. 1–3). We therefore investigated whether immunosuppression in this context would rather be under the control of another coinhibitory receptor, namely, TIM-3. To this aim, we first investigated the impact of TIM-3 expression on the functional properties of $CD8^+$ TILs from 20 freshly resected HGSCs (study group 2; Supplementary Table S1) using flow cytometry (Fig. 4A). Remarkably, about one third of tumor-infiltrating $CD8^+$ T cells expressed TIM-3 (mean 31.3%; SEM 32.6%), near to invariably in conjunction with PD-1. Nonspecific stimulation induced IFNγ production and CD107a exposure preferentially in TIM-3^-PD-1^- cells as compared with their TIM-3^+PD-1^+ counterparts ($P = 0.04$ and $P = 0.02$, respectively; Fig. 4B). Moreover, incubation with anti-TIM3 and anti–PD-1 antibodies (but not with either antibody alone) increased the ability of bulk tumor-infiltrating $CD8^+$ T cells to respond to nonspecific stimulation *in vitro* by synthetizing IFNγ and cytolytic molecules (i.e., GZMB, PRF1; study group 2; Fig. 4C). Thus, TIM-3^+PD-1^+ cells from the HGSC TME stand out as a functionally impaired $CD8^+$ T-cell subpopulation with limited effector functions.

We have previously shown that the intratumoral levels of PD-1^+ cells correlate with improved (rather than poor) disease outcome in chemotherapy-naïve HGSC patients (Fig. 1B and C), largely as they reflect $CD8^+$ CTL infiltration in this setting (Fig. 1D; Supplementary Fig. S8A). Thus, we interrogated the impact of tumor infiltration by TIM-3^+ cells on the immunologic profile of HGSCs and disease outcome. To this aim, we harnessed multispectral immunofluorescence staining combined with automated image analysis on a subset of 50 samples from study group 1 (Fig. 4D). In line with flow cytometry data (Fig. 4A), around 31.3% of the $CD8^+$ T cells infiltrating HGSC expressed TIM-3, most often in combination with PD-1 (Fig. 4E). We then selected 6 TIM-3^{Lo} patients and compared their transcriptional profile with that of 6 TIM-3^{Hi} individuals (study group 1). We identified 1,460 genes that were significantly overrepresented in samples from TIM-3^{Lo} patients relative to their TIM-3^{Hi} counterparts (Fig. 4F; Supplementary Table S7), and functional studies revealed a strong association between such DEGs and immune system activation and inflammation. Moreover, compared with their TIM-3^{Hi} counterparts, TIM-3^{Lo} tumors exhibited overrepresentation (rather than underrepresentation, as expected if TIM-3 behaved as a mere biomarker for T cells) of gene sets specific for $CD8^+$ T cells ($P = 0.04$), as determined by MCP-counter R package (Fig. 4G).

As we observed a negative correlation between infiltration by TIM-3^+ cells and the levels of several transcripts associated with T cells and immune system activation, we next evaluated the immunologic profile of the TME in TIM-3^{Lo} *versus* TIM-3^{Hi} tumors (as previously determined by multispectral immunofluorescence staining) by IHC (study group 1; Fig. 4H). This approach identified 4 different clusters of patients, which were characterized by either high levels of PD-L1 and extensive infiltration by $CD8^+$, PD-1^+, CTLA4$^+$, LAG-3^+, $CD20^+$, and DC-LAMP$^+$ cells (Immune^{Hi}) or the opposite situation (Immune^{Lo}), combined with abundant or limited infiltration by TIM-3 cells (Immune^{Hi}/TIM-3^{Hi}, Immune^{Hi}/TIM-3^{Lo}, Immune^{Lo}/TIM-3^{Hi}, and Immune^{Lo}/TIM-3^{Lo}; Fig. 4H).

Importantly, Immune^{Hi}/TIM-3^{Lo} patients had improved OS as compared with their Immune^{Hi}/TIM-3^{Hi} counterparts ($P = 0.04$), and so did Immune^{Lo}/TIM-3^{Lo} patients as compared with their Immune^{Lo}/TIM-3^{Hi} counterparts ($P = 0.04$; Fig. 4I). Such an effect could not be attributed to statistical differences in any parameter other than infiltration by TIM-3^+ cells within the Immune^{Hi} and Immune^{Lo} patient subgroups (Supplementary Table S8). Similarly, Immune^{Lo}/TIM-3^{Lo} patients had improved OS as compared with their Immune^{Lo}/TIM-3^{Hi} counterparts ($P = 0.04$; Fig. 4I). Univariate Cox regression confirmed the negative prognostic impact of tumor infiltration by TIM-3^+ cells (HR = 1.03; 95% confidence interval = 1.00–1.06; $P = 0.04$; Table 2), and the significance of this association was validated by multivariate analysis (HR = 1.41; 95% confidence interval = 1.1–1.9; $P = 0.03$) (Table 3). To corroborate our findings in an independent patient cohort, we retrieved normalized *HAVCR2* levels (TIM-3) for 308 patients with HGSC from the TCGA database and stratified these them into 4 groups based on TIM-3 expression and the expression of genes linked to $CD8^+$ T cells (*CD8A*), DCs (*LAMP3*, which codes for DC-LAMP) and B cells (*MS4A1*). Also in this setting, Immune^{Hi}/TIM-3^{Lo} had improved OS as compared with their Immune^{Hi}/TIM-3^{Hi} counterparts ($P = 0.04$; Fig. 4I). Altogether, these findings document a critical role for TIM-3 in the establishment of clinically relevant immunosuppression in TME of patients with HGSC.

Discussion

Coinhibitory receptors expressed on T cells play a major role in the establishment of clinically relevant immunosuppression

Downloaded from http://aacrjournals.org/clincancerres/article-pdf/25/15/4820/2051487/4820.pdf by guest on 23 May 2025

Figure 4.

TIM-3 dictates clinically relevant immunosuppression in the TME of HGSC. **A,** Gating strategy for TIM-3^+PD-1^+ TIM-3^-PD-1^- cells (study group 2). The percentage of cells in each gate is reported. **B,** Percentage of IFNγ$^+$ and CD107$^+$ $CD8^+$ T cells among TIM-3^+PD-1^+ and TIM-3^-PD-1^- $CD8^+$ T cells. **C,** Fold change of IFNγ$^+$ and PRF1/GZMB$^+$ $CD8^+$ T cells after incubation with anti–PD-1, anti–TIM-3, and combination of anti–PD-1/anti–TIM-3 antibodies (study group 2). **D,** Representative images of CD8, PD-1, and TIM-3 multispectral immunofluorescence (left). Cells expressing CD8 (red arrow), cells coexpressing CD8 and PD-1 (yellow arrow), and cells coexpressing CD8, PD-1, and TIM-3 (violet arrow). For automated counting, inForm software allows cell segmentation based on DAPI staining of the nucleus and morphometric characteristics (right). **E,** Percentage of TIM-3^+PD-1^-, TIM-3^+PD-1^+, TIM-3^-PD-1^+, and TIM-3^-PD-1^- $CD8^+$ T cells as determined by *in situ* immunofluorescence in study group 1. **F,** Hierarchical clustering of 1,460 transcripts that were significantly changed in 6 TIM-3^{Hi} patients as compared with their 6 TIM-3^{Lo} counterparts from study group 1, as determined by RNA-sequencing. **G,** Relative expression levels of gene sets associated with $CD8^+$ T cells across TIM-3^{Hi} and TIM-3^{Lo} HGSCs, as determined by MCP-counter on RNA-seq data from study group 1. Box plots: lower quartile, median, upper quartile; whiskers, minimum, maximum. **H,** Clustering of 50 HGSC patients from study group 1 based on densities of PD-1^+, LAG-3^+, CTLA-4^+, PD-L1^+, $CD8^+$, DC-LAMP$^+$, $CD20^+$, and TIM-3^+ cells as determined by IHC and multispectral immunofluorescence. **I,** OS of 50 and 308 HGSC patients from study group 1 and the TCGA public database who did not receive neoadjuvant chemotherapy, upon stratification based on the median density of TIM-3^+ cells and immune infiltrate as indicated by clustering heat map. Survival curves were estimated by the Kaplan–Meier method, and differences between groups were evaluated using the log-rank test. The number of patients at risk is reported.

in the microenvironment of most (if not all) human malignancies (28–30). Consistent with this notion, immune-checkpoint blockers that prevent the binding of coinhibitory receptors with their cognate ligands mediate robust clinical efficacy in subsets of patients affected by melanoma, NSCLC, and urothelial carcinoma (31). This is especially true when coinhibitory ligands such as PD-L1 are highly expressed in the TME (3, 4, 28). Recent data indicate that PD-L1$^+$ ovarian cancer patients may also obtain clinical benefits from PD-1-targeting immune-checkpoint blockers (32), reinstating the value of PD-L1 as a predictive biomarker for preselecting patients who are likely to respond to immunotherapies targeting the PD-1/PD-L1 axis.

The predictive value of PD-L1 has largely been attributed to its ability to identify tumors with active PD-1 signaling (33). Here, we demonstrate that high levels of PD-L1 are associated with improved disease outcome among chemotherapy-naïve (and immunotherapy-naïve) HGSC patients (Fig. 1), implying that the prognostic value of PD-L1 in our cohort of patients cannot be attributed to its ability to identify a therapeutic target for PD-1 blockers. Rather, our data suggest that high PD-L1 levels constitute a biomarker for spontaneous IFNγ-mediated antitumor immunity (Fig. 2). Consistent with this interpretation, HGSC patients with robust tumor infiltration by CD8$^+$ T cells, but low levels of PD-L1 exhibited remarkably poor disease outcome as compared with patients with high levels of tumor-infiltrating T cells but high PD-L1 expression in the TME (Fig. 2). Moreover, tumor infiltration by T cells expressing coinhibitory receptors such as PD-1, CTLA4, and LAG-3 was associated with superior (rather than inferior) RFS and OS (Fig. 1), and neither of these parameters was able to improve patient stratification based on the intratumoral levels of CD8$^+$ T cells only, with the possible exception of CTLA4 (Supplementary Fig. S8A–S8C). Thus, in the TME of chemotherapy-naïve HGSC patients, PD-1 and LAG-3 largely behave as biomarkers of infiltration by CD8$^+$ T cells (Fig. 1D; Supplementary Fig. S8A–S8C), while PD-L1 expression identifies a clinically relevant, spontaneous anticancer immune response. To our surprise, a low density of CTLA4$^+$ cells appears to identify a subgroup of CD8^{Hi} HGSC patients with relatively poor (rather than good) disease outcome as compared with their CD8^{Hi}CTLA^{Hi} counterparts. Potentially, such an unexpected finding may either reflect the expression of CTLA4 by myeloid cells supporting antitumor immunity (34) or originate from the relatively low number of patients in the CD8^{Hi}CTLA4^{Lo} group.

We were surprised to find that neither of the major coinhibitory receptors we analyzed at first was associated with an independent negative prognostic value in our patient cohort, which led us to refocus our attention on the comparatively less known molecule TIM-3. We found that one third of CD8$^+$ T cells that infiltrate chemotherapy-naïve HGSCs express TIM-3, generally in association with PD-1 (Fig. 4A and E). Not only such TIM-3$^+$PD-1$^+$ cells exhibit signs of functional exhaustion, both at baseline and upon nonspecific stimulation (Fig. 4B and C), but their abundance conveys a negative independent prognostic value that can be harnessed to obtain improved patient stratification (Fig. 4I). Moreover, only CD8$^+$ T cells from TIM-3^{Hi} (but not TIM-3^{Lo}) patients are sensitive to TIM-3 blockade (in combination with PD-1, but not CTLA4, blockade; Supplementary Fig. S8D). These findings are in line with data from other groups identifying the negative impact of TIM-3 expression on tumor-infiltrating CD8$^+$ T cells in multiple oncological settings (27, 35–38). Moreover, they suggest that targeting TIM-3 with immune-checkpoint blockers may be a particularly promising approach for the treatment of HGSC. To the best of our knowledge, although multiple clinical trials are currently assessing the therapeutic profile of TIM-3-targeting agents in open-label settings, no study specifically testing TIM-3 inhibitors in ovarian cancer patients is currently recruiting participants (source: www.clinicaltrials.gov).

In conclusion, our findings demonstrate that PD-L1 and TIM-3 are biomarkers of active and suppressed, respectively, spontaneous immunity against HGSC. Besides identifying in TIM-3 a potentially actionable target for the treatment of HGSC patients, these data suggest that the ability of PD-L1 expression levels to identify patients who are likely to respond to PD-1– or PD-L1–targeting agents may reflect (at least to some extent or in some setting) the preexistence of a natural immune response against the tumor.

Disclosure of Potential Conflicts of Interest

L. Galluzzi is a consultant/advisory board member for Astra Zeneca, OmniSEQ, and The Luke Heller Foundation, and reports receiving commercial research grants from Lytix and Phosplatin. No potential conflicts of interest were disclosed by the other authors.

Authors' Contributions

Conception and design: J. Fucikova, J. Laco, L. Galluzzi, R. Spisek
Development of methodology: J. Fucikova, M. Hensler, L. Kasikova, L. Belicova, J. Pineau, A. Gey, E. Tartour
Acquisition of data (provided animals, acquired and managed patients, provided facilities, etc.): J. Fucikova, J. Rakova, M. Hensler, L. Kasikova, L. Belicova, K. Hladikova, P. Skapa, J. Laco, I. Praznovec, M.J. Halaska, T. Brtnicky, R. Kodet, J. Pineau, A. Gey, E. Tartour, A. Ryska
Analysis and interpretation of data (e.g., statistical analysis, biostatistics, computational analysis): J. Fucikova, J. Rakova, M. Hensler, L. Kasikova, L. Belicova, K. Hladikova, L. Pecen, A. Fialova, J. Pineau, A. Gey, E. Tartour, L. Galluzzi
Writing, review, and/or revision of the manuscript: J. Fucikova, L. Kasikova, I. Truxova, P. Skapa, M.J. Halaska, J. Pineau, A. Gey, E. Tartour, A. Ryska, L. Galluzzi, R. Spisek
Administrative, technical, or material support (i.e., reporting or organizing data, constructing databases): J. Fucikova, J. Rakova, L. Kasikova
Study supervision: J. Fucikova, L. Galluzzi, R. Spisek

Acknowledgments

This study was exclusively sponsored by Sotio, Prague, Czech Republic. This study was supported by program PROGRES Q40/11, by the project BBMRI-CZ LM2015089, and by the European Regional Development Fund-Project BBMRI-CZ.: Biobank network—a versatile platform for research on the etiopathogenesis of diseases, No: EF16 013/0001674. L. Galluzzi is supported by a Breakthrough Level 2 grant from the US Department of Defense (DoD), Breast Cancer Research Program (BRCP; #BC180476P1), by a startup grant from the Department of Radiation Oncology at Weill Cornell Medicine (New York), by industrial collaborations with Lytix (Oslo, Norway) and Phosplatin (New York), and by donations from Phosplatin (New York), the Luke Heller TECPR2 Foundation (Boston) and Sotio a.s. (Prague, Czech Republic).

The costs of publication of this article were defrayed in part by the payment of page charges. This article must therefore be hereby marked *advertisement* in accordance with 18 U.S.C. Section 1734 solely to indicate this fact.

Received December 20, 2018; revised March 19, 2019; accepted May 9, 2019; published first May 10, 2019.

Downloaded from http://aacrjournals.org/clincancerres/article-pdf/25/15/4820/2051487/4820.pdf by guest on 23 May 2025

References

1. Fridman WH, Zitvogel L, Sautes-Fridman C, Kroemer G. The immune contexture in cancer prognosis and treatment. Nat Rev Clin Oncol 2017;14: 717–34.
2. Galon J, Costes A, Sanchez-Cabo F, Kirilovsky A, Mlecnik B, Lagorce-Pages C, et al. Type, density, and location of immune cells within human colorectal tumors predict clinical outcome. Science 2006;313:1960–4.
3. Skov BG, Kiss K, Ramsted J, Linnemann D. A technique to improve diagnostic information from fine-needle aspirations: immunohistochemistry on cytoscrape. Cancer 2009;117:120–7.
4. Passiglia F, Bronte G, Bazan V, Natoli C, Rizzo S, Galvano A, et al. PD-L1 expression as predictive biomarker in patients with NSCLC: a pooled analysis. Oncotarget 2016;7:19738–47.
5. Truxova I, Kasikova L, Hensler M, Skapa P, Laco J, Pecen L, et al. Mature dendritic cells correlate with favorable immune infiltrate and improved prognosis in ovarian carcinoma patients. J Immunother Cancer 2018;6: 139.
6. Chen DS, Mellman I. Elements of cancer immunity and the cancer-immune set point. Nature 2017;541:321–30.
7. Savas P, Salgado R, Denkert C, Sotiriou C, Darcy PK, Smyth MJ, et al. Clinical relevance of host immunity in breast cancer: from TILs to the clinic. Nat Rev Clin Oncol 2016;13:228–41.
8. Hamanishi J, Mandai M, Iwasaki M, Okazaki T, Tanaka Y, Yamaguchi K, et al. Programmed cell death 1 ligand 1 and tumor-infiltrating CD8+ T lymphocytes are prognostic factors of human ovarian cancer. Proc Natl Acad Sci U S A 2007;104:3360–5.
9. Webb JR, Milne K, Kroeger DR, Nelson BH. PD-L1 expression is associated with tumor-infiltrating T cells and favorable prognosis in high-grade serous ovarian cancer. Gynecol Oncol 2016;141:293–302.
10. Taube JM, Anders RA, Young GD, Xu H, Sharma R, McMiller TL, et al. Colocalization of inflammatory response with B7-h1 expression in human melanocytic lesions supports an adaptive resistance mechanism of immune escape. Sci Transl Med 2012;4:127ra37.
11. Schalper KA, Velcheti V, Carvajal D, Wimberly H, Brown J, Pusztai L, et al. In situ tumor PD-L1 mRNA expression is associated with increased TILs and better outcome in breast carcinomas. Clin Cancer Res 2014;20:2773–82.
12. Lipson EJ, Vincent JG, Loyo M, Kagohara LT, Luber BS, Wang H, et al. PD-L1 expression in the Merkel cell carcinoma microenvironment: association with inflammation, Merkel cell polyomavirus and overall survival. Cancer Immunol Res 2013;1:54–63.
13. D'Angelo SP, Shoushtari AN, Agaram NP, Kuk D, Qin LX, Carvajal RD, et al. Prevalence of tumor-infiltrating lymphocytes and PD-L1 expression in the soft tissue sarcoma microenvironment. Hum Pathol 2015;46:357–65.
14. Muenst S, Soysal SD, Gao F, Obermann EC, Oertli D, Gillanders WE. The presence of programmed death 1 (PD-1)-positive tumor-infiltrating lymphocytes is associated with poor prognosis in human breast cancer. Breast Cancer Res Treat 2013;139:667–76.
15. Thompson RH, Dong H, Lohse CM, Leibovich BC, Blute ML, Cheville JC, et al. PD-1 is expressed by tumor-infiltrating immune cells and is associated with poor outcome for patients with renal cell carcinoma. Clin Cancer Res 2007;13:1757–61.
16. Giraldo NA, Becht E, Pages F, Skliris G, Verkarre V, Vano Y, et al. Orchestration and prognostic significance of immune checkpoints in the microenvironment of primary and metastatic renal cell cancer. Clin Cancer Res 2015;21:3031–40.
17. Badoual C, Hans S, Merillon N, Van Ryswick C, Ravel P, Benhamouda N, et al. PD-1-expressing tumor-infiltrating T cells are a favorable prognostic biomarker in HPV-associated head and neck cancer. Cancer Res 2013;73: 128–38.
18. Takahashi H, Tomita N, Sakata S, Tsuyama N, Hashimoto C, Ohshima R, et al. Prognostic significance of programmed cell death-1-positive cells in follicular lymphoma patients may alter in the rituximab era. Eur J Haematol 2013;90:286–90.
19. Webb JR, Milne K, Nelson BH. PD-1 and CD103 are widely coexpressed on prognostically favorable intraepithelial CD8 T cells in human ovarian cancer. Cancer Immunol Res 2015;3:926–35.
20. O'Sullivan B, Brierley J, Byrd D, Bosman F, Kehoe S, Kossary C, et al. The TNM classification of malignant tumours-towards common understanding and reasonable expectations. Lancet Oncol 2017;18:849–51.
21. Meinhold-Heerlein I, Fotopoulou C, Harter P, Kurzeder C, Mustea A, Wimberger P, et al. The new WHO classification of ovarian, fallopian tube, and primary peritoneal cancer and its clinical implications. Arch Gynecol Obstet 2016;293:695–700.
22. Solomon B, Young RJ, Bressel M, Urban D, Hendry S, Thai A, et al. Prognostic significance of PD-L1(+) and CD8(+) immune cells in HPV(+) oropharyngeal squamous cell carcinoma. Cancer Immunol Res 2018. doi: 10.1158/2326-6066.CIR-17-0299. [Epub ahead of print].
23. Becht E, Giraldo NA, Lacroix L, Buttard B, Elarouci N, Petitprez F, et al. Estimating the population abundance of tissue-infiltrating immune and stromal cell populations using gene expression. Genome Biol 2016;17: 218.
24. Ritchie ME, Phipson B, Wu D, Hu Y, Law CW, Shi W, et al. limma powers differential expression analyses for RNA-sequencing and microarray studies. Nucleic Acids Res 2015;43:e47.
25. Gu Z, Eils R, Schlesner M. Complex heatmaps reveal patterns and correlations in multidimensional genomic data. Bioinformatics 2016; 32:2847–9.
26. Bindea G, Mlecnik B, Hackl H, Charoentong P, Tosolini M, Kirilovsky A, et al. ClueGO: a Cytoscape plug-in to decipher functionally grouped gene ontology and pathway annotation networks. Bioinformatics 2009;25: 1091–3.
27. Granier C, Dariane C, Combe P, Verkarre V, Urien S, Badoual C, et al. Tim-3 expression on tumor-infiltrating PD-1(+)CD8(+) T cells correlates with poor clinical outcome in renal cell carcinoma. Cancer Res 2017;77: 1075–82.
28. Topalian SL, Drake CG, Pardoll DM. Immune checkpoint blockade: a common denominator approach to cancer therapy. Cancer Cell 2015;27: 450–61.
29. Pardoll DM. The blockade of immune checkpoints in cancer immunotherapy. Nat Rev Cancer 2012;12:252–64.
30. Tumeh PC, Harview CL, Yearley JH, Shintaku IP, Taylor EJ, Robert L, et al. PD-1 blockade induces responses by inhibiting adaptive immune resistance. Nature 2014;515:568–71.
31. Vanpouille-Box C, Lhuillier C, Bezu L, Aranda F, Yamazaki T, Kepp O, et al. Trial watch: Immune checkpoint blockers for cancer therapy. Oncoimmunology 2017;6:e1373237.
32. Varga A, Piha-Paul S, Ott PA, Mehnert JM, Berton-Rigaud D, Morosky A, et al. Pembrolizumab in patients with programmed death ligand 1-positive advanced ovarian cancer: analysis of KEYNOTE-028. Gynecol Oncol 2018;(152:243–50.
33. Sharpe AH, Pauken KE. The diverse functions of the PD1 inhibitory pathway. Nat Rev Immunol 2018;18:153–67.
34. Halpert MM, Konduri V, Liang D, Chen Y, Wing JB, Paust S, et al. Dendritic cell-secreted cytotoxic T-lymphocyte-associated protein-4 regulates the T-cell response by downmodulating bystander surface B7. Stem Cells Dev 2016;25:774–87.
35. Hladikova K, Partlova S, Koucky V, Boucek J, Fonteneau JF, Zabrodsky M, et al. Dysfunction of HPV16-specific CD8+ T cells derived from oropharyngeal tumors is related to the expression of Tim-3 but not PD-1. Oral Oncol 2018;82:75–82.
36. Zhou Q, Munger ME, Veenstra RG, Weigel BJ, Hirashima M, Munn DH, et al. Coexpression of Tim-3 and PD-1 identifies a CD8+ T-cell exhaustion phenotype in mice with disseminated acute myelogenous leukemia. Blood 2011;117:4501–10.
37. Shayan G, Srivastava R, Li J, Schmitt N, Kane LP, Ferris RL. Adaptive resistance to anti-PD1 therapy by Tim-3 upregulation is mediated by the PI3K-Akt pathway in head and neck cancer. Oncoimmunology 2017;6: e1261779.
38. Sakuishi K, Apetoh L, Sullivan JM, Blazar BR, Kuchroo VK, Anderson AC. Targeting Tim-3 and PD-1 pathways to reverse T cell exhaustion and restore anti-tumor immunity. J Exp Med 2010;207:2187–94.

Downloaded from http://aacrjournals.org/clincancerres/article-pdf/25/15/4820/2051487/4820.pdf by guest on 23 May 2025